





Article

Temperature and Pressure Dependence of the Infrared Spectrum of 1-Ethyl-3-Methylimidazolium Trifluoromethanesulfonate Ionic Liquid

Francesco Trequattrini ^{1,2}, Anna Celeste ^{3,4}, Francesco Capitani ⁴, Oriele Palumbo ^{2,*},
Adriano Cimini ² and Annalisa Paolone ²

¹ Dipartimento di Fisica, Sapienza Università di Roma, Piazzale A. Moro 5, 00185 Roma, Italy; francesco.trequattrini@roma1.infn.it

² Consiglio Nazionale delle Ricerche-Istituto dei Sistemi Complessi, U.O.S. La Sapienza, Piazzale A. Moro 5, 00185 Roma, Italy; cimini.1233261@studenti.uniroma1.it (A.C.); annalisa.paolone@roma1.infn.it (A.P.)

³ Institut de Chimie et des Matériaux Paris-Est, CNRS UMR 7182, UPEC, 2-8, rue Henri Dunant, 94320 Thiais, France; anna.celeste@synchrotron-soleil.fr

⁴ Synchrotron SOLEIL, L'Orme des Merisiers, 91192 Saint-Aubin, Gif sur Yvette CEDEX, France; francesco.capitani@synchrotron-soleil.fr

* Correspondence: oriele.palumbo@roma1.infn.it; Tel.: +39-06-4991-4400

Received: 13 May 2020; Accepted: 24 June 2020; Published: 26 June 2020



Abstract: The infrared absorption spectrum of 1-ethyl-3-methylimidazolium trifluoromethanesulfonate (EMI-TfO) was investigated at ambient pressure and variable temperatures between 120 and 330 K, or at room temperature and variable pressures up to 10 GPa. Upon cooling, the ionic liquid crystallizes; on the contrary, upon compression no evidence of crystallization can be obtained from the infrared spectra. Moreover, Density Functional Theory (DFT) calculations were applied to gain a better description of the ionic couple. The ω B97X-D functional, including not only the empirical dispersion corrections but also the presence of a polar solvent, gives a good agreement with the infrared spectrum and suggests that TfO resides above the plane of the imidazolium, with the shorter distance between the O atom of the anion and the C2 atom of the imidazolium ring equal to 2.23 Å.

Keywords: infrared spectroscopy; diamond anvil cell; DFT calculations; ionic couple

1. Introduction

Ionic liquids (ILs) have attracted huge attention in the last years for their potential applications in a large variety of fields: as solvents [1], sorbents of dangerous or hazardous gases [2], components of microemulsions [3] or extraction [4] or microextraction systems [5], vehicles for drug delivery [6], thermally responsive materials [7], activation agents for biocatalysis [8] or components of electrolytes for electrochemical devices [9,10].

At the basis of the versatility of ILs, there is the possibility to combine a large number of anions and cations to optimize an IL to the desired property. Usually, the cations are organic ions, such as imidazolium, pyrrolidinium, alkyl ammonium or phosphonium, while the anions can be inorganic or organic ions, such as tetrafluoroborate (BF_4), hexafluorophosphate (PF_6), dicyanamide (DCA), tetracyanamethanide ($\text{B}(\text{CN})_4$), trifluoromethanesulfonate (TfO, also known as triflate), bis(trifluoromethanesulfonyl)imide (TFSI) or bis(fluorosulfonyl)imide (FSI). In addition, it is possible to combine two or more ILs together [11] or with solvents, so that an incredible number of combinations are envisaged.

Vibrational spectroscopies, such as infrared or Raman, are powerful investigation techniques of the internal structure of ILs and of the possible phase transitions that ILs can undergo as a function

of temperature or pressure. Many experimental and computational studies in this field have been summarized in a recent review [12]. The exploitation of temperature and pressure dependence of physical properties is not equivalent from the thermodynamic point of view because pressure mainly induces a variation of density, whereas temperature varies kinetic energy and density simultaneously [13,14]. Indeed, many ILs display different behaviors as a function of temperature or pressure [15–26]; for example, some ILs that crystallize upon cooling transform, instead, into a glass state at high pressure. It must be noted that when pressure is applied, a compression is induced, the intermolecular distances decrease and the material can experience the repulsive part of the intermolecular potential, which is not accessible by a change of temperature [27].

Moreover, useful information is obtained by the comparison of experimental data with computational results, which are easily obtained in the case of ionic liquids. A high valuable consequence of this approach is that calculations can indicate strategies for the synthesis of ILs with specific properties, avoiding a simple “trial and error” process. Several reviews [28,29] reported on the progress of multiscale calculations starting from the knowledge of the single ions composing an IL to calculate macroscopic physical quantities, such as viscosity, decomposition temperatures and ionic conductivity, or to predict how to design a reactor or a whole process based on ILs.

Density Functional Theory (DFT) calculations are commonly used to investigate the molecular structure of compounds or ions and have been largely used for the study of ILs [12]. One of the results of these kinds of calculations are the vibrational frequencies and the infrared and Raman intensities, which can be easily compared to experiments. For many years, DFT studies were devoted to the investigations of single cations or anions and to the occurrence of their conformers [30–34]. More recently, calculations performed on ionic couples or on a limited number of ionic couples have become more easily accessible from a computational point of view, providing important information about the interactions between anion and cation and among ionic couples [35,36]. In particular, concerning intermolecular interactions, interesting information has been obtained about the occurrence of hydrogen bonding [37–41]. Subtle changes in the vibrational spectra can be associated to specific interactions. However, it is important to determine which DFT model is able to better describe the interionic interactions.

In this context, we attempted to gain a better knowledge of the phase diagram of a simple ionic liquid, namely 1-ethyl-3-methylimidazolium trifluoromethanesulfonate. Compared to other ILs, trifluoromethanesulfonate (also known as triflate)-based ionic liquids are hydrolytically stable and are preferred as reaction media to the hydrolytically unstable PF_6 and BF_4 anions [42]. Moreover, they are able to polymerize methyl methacrylate [43] with an extremely high molecular weight. They are highly thermally and electrochemically stable and are potentially interesting for heat transfer materials, lubricants and as components of electrolytes for electrochemical cells [44]. For the presently investigated IL, we performed infrared spectroscopy measurements at ambient pressure as a function of T , and at room temperature with increasing pressure. We evidence that at low temperatures the IL crystallizes, while with high pressure it does not. Moreover, the comparison of a computational investigations of the single ions and of an ionic couple by means of DFT calculations indicates that the infrared spectrum can be better described considering together the anion and cation using the $\omega\text{B97X-D}$ functional, both considering the empirical dispersion corrections and the presence of a polar solvent.

2. Materials and Methods

1-Ethyl-3-methylimidazolium trifluoromethanesulfonate (EMI-TfO) with a purity of 99% was purchased from Iolitec. A scheme of the ions composing the ionic liquid is reported in Figure 1. To avoid contaminations of undesired water from the atmosphere, the sample was stored in a glove box filled with pure Ar. Before the infrared measurements, the sample was additionally heated in a vacuum of the order of 10^{-5} mbar for 48 h at about 80 °C to remove eventual water contaminations.

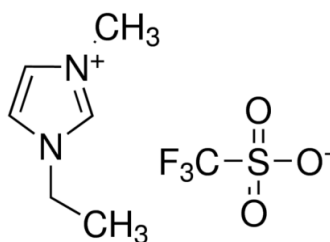


Figure 1. Scheme of the cation and anion composing the investigated ionic liquid.

Infrared absorbance measurements were conducted as a function of temperature in the range of 120–330 K at the AILES beamline of Soleil Synchrotron, by means of a Bruker IFS125 HR spectrometer with a resolution of 1 cm^{-1} . A few droplets of the neat sample were placed between the two diamond optical windows of a vacuum-sealed cell for liquids. The temperature was varied by the Cryomech cryostat available at AILES with a temperature rate of 5 K/min. The spectra were recorded in the mid-infrared range using a KBr beam splitter and a wide range low noise MCT [45]; in the far-infrared range, spectra were acquired by means of a Si-coated mylar beamsplitter and a bolometer.

Absorbance measurements as a function of pressure at room temperature were performed at the SMIS beamline of Soleil Synchrotron, by means of a Nicolet iS50 spectrometer (Thermo-Fisher, Waltham, MA, USA) coupled with a home-made horizontal microscope dedicated to high-pressure experiments. The microscope has custom long working distance Schwarzschild objectives which allowed performing transmittance measurements in the diamond anvil cell (DAC). Spectra were recorded in the mid-infrared range with a KBr beamsplitter and a resolution of 1 cm^{-1} . DAC was equipped with diamond anvils of type IIa with a culet diameter of $400\text{ }\mu\text{m}$ and a stainless steel gasket pre-indented to a thickness of $50\text{ }\mu\text{m}$, where a hole of $150\text{ }\mu\text{m}$ was drilled to be used as a sample chamber. NaCl was used as a pressure-transmitting medium and to reduce the sample thickness and avoid signal saturation [46]. Pressure was measured in-situ through the standard ruby luminescence technique [47]. The luminescence was excited and collected using a home-built optical setup aligned with the Schwarzschild objectives and made of dichroic mirrors, a 532 nm green laser, a camera, a lamp and a fiber collimator connected to an Ocean Optics HR4000 spectrometer. Before acquiring each spectrum, we waited for about five minutes to achieve pressure stabilization.

All calculations were performed by means of the Spartan software [48]. Possible geometries were generated at the molecular mechanics level. All structures were afterwards optimized by means of DFT calculations. For the single ions EMI and TfO, the B3LYP functional was employed considering the ions as isolated in vacuum; this particular functional is considered as a benchmark for this type of calculation [12]. For the ionic couple EMI–TfO, the ω B97X-D functional, considering both the empirical dispersion corrections and the presence of a polar solvent (dimethylformamide, $\epsilon_r = 37.22$), was used. Indeed, this last combination of functional, dispersion forces and polar solvent has recently provided a good description of the absorbance spectra of diethyl methyl ammonium methanesulfonate (DEMA-MS) and diethyl methyl ammonium trifluoromethanesulfonate (DEMA-TfO) [49]. The introduction of the polar solvents represents a further improvement compared to previous similar DFT calculations [35–50]. For all calculations, the 6-31G** basis set was used. After optimization of the geometry of single ions or of the ionic couple, the infrared vibrational frequencies and intensities were obtained with the same level of theory and basis set adopted for the optimization. To compare the experimental infrared spectrum with the simulated ones, we produced simulated infrared spectra adding Gaussian curves with maximum at each calculated vibration frequency, a 10 cm^{-1} line width and an intensity proportional to the calculated one.

3. Results and Discussion

3.1. Absorbance as a Function of Temperature

Figure 2 reports the infrared absorption spectrum of EMI-TfO measured on cooling from 330 K down to 120 K and subsequent heating from 120 K up to 330 K, in the frequency range between 500 and 1800 cm^{-1} . In all spectra, the most intense lines centered around 518, 574, 638, 1031, 1167, 1226, 1266 cm^{-1} are known to be due to the vibrations of the TfO anions [49]. The less intense lines between 680 and 1000 cm^{-1} , as well as the absorption bands above 1300 cm^{-1} , are due to the vibration modes of the EMI cation [32].

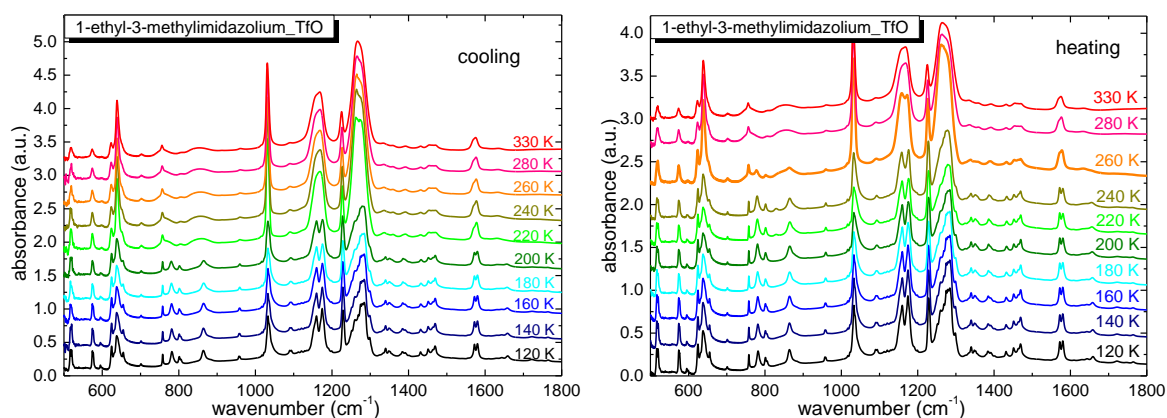


Figure 2. Absorbance of 1-Ethyl-3-methylimidazolium trifluoromethanesulfonate (EMI-TfO) in the mid infrared range, measured on cooling (**left panel**) and subsequent heating (**right panel**).

On cooling, small modifications of the absorption spectrum are detected between 330 and 220 K; however, between 220 and 200 K an abrupt change takes place, consisting in the splitting of the lines between 730 and 820 cm^{-1} , and between 1150 and 1600 cm^{-1} . On further cooling, the spectral features remain constant. On subsequent heating (see Figure 2 right panel), minor modifications occur up to 260 K; at this temperature, the absorption lines start to become less defined: the band around 1590 cm^{-1} stops being a well defined doublet and resembles more the broad band observed on cooling in the liquid phase; but, on the other hand, one can still observe the three bands between 740 and 820 cm^{-1} , that are, instead, a broad feature in the liquid. The strong absorption bands between 1000 and 1300 cm^{-1} become more intense than in the solid phase at low temperature and in the liquid one at high temperature. On further increasing the temperature, around 280 K all absorption bands return to the shape they had in the liquid phase at room temperature before the thermal cycle. The splitting of absorption bands or the abrupt disappearance or appearance of spectral lines has been largely attributed to the occurrence of solid–liquid or solid–solid transformations [12–26,49]. In this framework, the overall behavior as a function of temperature of EMI-TfO can be attributed to the occurrence of crystallization on cooling between 220 and 200 K and the occurrence of a solid–solid phase transition on heating around 260 K and finally to melting around 280 K. Indeed, this phase changes are in agreement with differential scanning calorimetry measurements reported in Ref. [51], which evidenced the occurrence of crystallization on cooling around 220 K, a subsequent solid–solid phase transition on heating around 230 K and melting around 260 K.

3.2. Absorbance as a Function of Pressure

Figure 3 displays the evolution of the infrared absorption between 600 and 1500 cm^{-1} as a function of pressure in the range 0.1–10 GPa. Note that a background of interference fringes, due to multiple reflections between the two parallel diamond surfaces, is present over the whole spectral and pressure range. At low pressures, one can clearly observe the intense absorption

lines of the anion centered around 639, 1031, 1163, 1225 and 1263 cm^{-1} , similar to the same bands measured at 330 K in the temperature-dependent experiments, which are reported for comparison in the lower part of Figure 3. Concerning the cation vibrations, one can observe the line around 758 cm^{-1} and the CH bending bands above 1300 cm^{-1} . With the increasing of the applied pressure, p , all bands shift towards higher frequencies, as expected, except for the absorption band centered around 639 cm^{-1} , that corresponds to the SO bond vibration [35]. This fact can be ascribed to a high strength of the SO double bond; such resilience to frequency shift of the SO vibration around 630 cm^{-1} was observed also in *N*-trimethyl-*N*-propylammoniumbis(trifluoromethanesulfonyl)imide and *N*-trimethyl-*N*-hexylammoniumbis(trifluoromethanesulfonyl)imide, whose TFSI anion has two SO_2 groups with the same type of vibrations around 620 cm^{-1} [23].

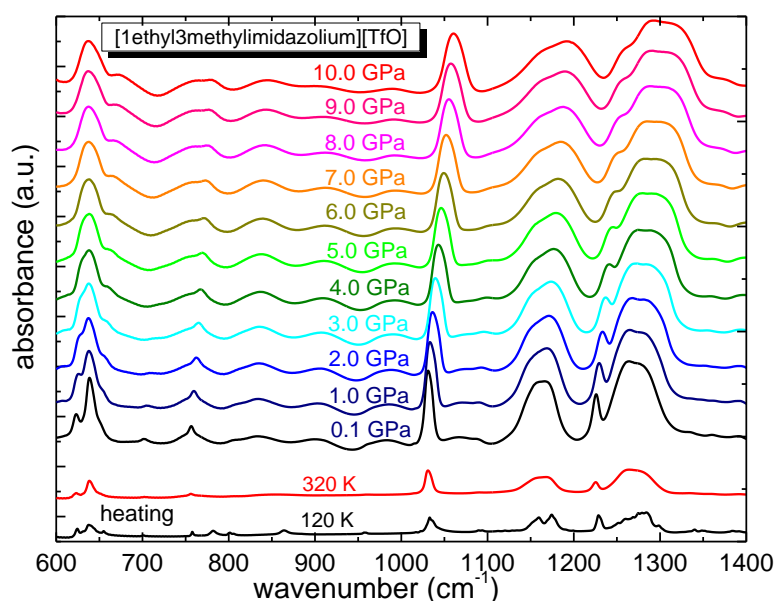


Figure 3. Absorbance of EMI-TfO in the mid infrared range measured at room temperature as a function of pressure. For comparison, two spectra recorded as a function of the temperature on heating in the same frequency range are reported in the lower part of the figure.

With increasing p , no splitting nor any abrupt disappearance of absorption lines is visible, suggesting that the sample does not undergo a crystallization process. In the literature, the occurrence of phase transitions as a function of pressure has been revealed in some cases by a change of the slope of the position of absorption peaks as a function of applied pressure. Most of the intense absorptions reported in Figure 3 do not appear as single bands, as they are composed by multiple contributions. Only the absorption line centered around 1031 cm^{-1} for $p = 0.1$ GPa can be assimilated to a single band. A fit with a single Lorentzian curve for this contribution has been performed for all the measured pressure spectra and Figure 4 reports the frequency of such a vibration band, ν_b , as a function of p . It is well evident that the slope remains constant on the whole pressure range here investigated. Therefore, it seems unlikely that the sample undergoes any crystallization as a function of pressure. This behavior is quite different from the temperature dependence, which, on the contrary, indicates the transformation towards a crystalline state at low temperatures. By a fit of the data reported in Figure 4, one obtains a variation of the vibration frequency versus applied pressure of $\partial\nu_b/\partial p = 3.04 \pm 0.02 \text{ cm}^{-1}\cdot\text{GPa}^{-1}$. This value is close to those reported for 1-decyl-3-methylimidazolium tetrafluoroborate, 1-octyl-3-methylimidazolium tetrafluoroborate, 1-butyl-2,3-dimethylimidazolium tetrafluoroborate, 1-butyl-1-methylpyrrolidinium tetrafluoroborate and 1-hexyl-3-methylimidazolium tetrafluoroborate [15,52,53].

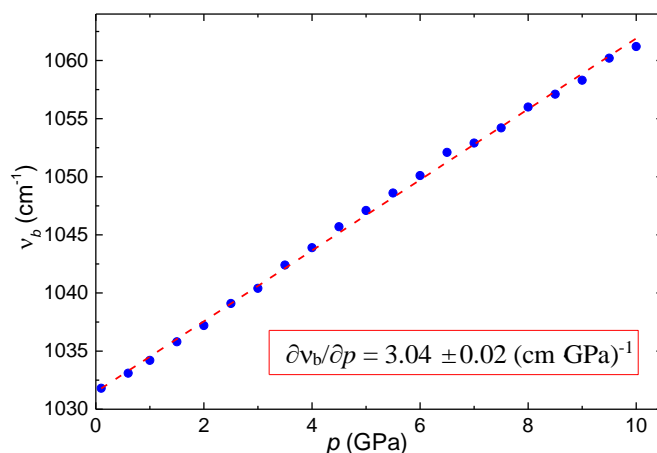


Figure 4. Dependence of the frequency of the vibration mode centered at 1031 cm^{-1} at 0.1 GPa from the applied pressure.

To the best of our knowledge, only a couple of reports about the pressure phase diagram of TfO-based ILs are available [52,54,55]. It has been reported that the ionic liquids having 1-butyl-3-methylimidazolium and 1-butyl-1-methylpyrrolidinium as cations crystallize around 1.0 GPa when the pressure is increased in steps of ~ 0.2 GPa from atmospheric pressure; on the contrary, the ILs containing the cations 1-octyl-3-methylimidazolium and 1-butyl-2,3-dimethylimidazolium do not crystallize up to 2.3 GPa. Moreover, in 1-butyl-3-methylimidazolium trifluoromethanesulfonate, the symmetry of the line at 1032 cm^{-1} , attributed to the symmetric stretching motions of the S–O bonds, was interpreted as originating from TO–LO splitting of the vibrational mode [55]. In this case, the experimental results were shown to follow the general predictions of dipolar coupling theory, thus confirming the quasi lattice model for this ionic liquid.

For the sake of completeness, we would like to point out that the kinetics of phase transitions can be sluggish, sometimes even longer than typical IR measurements. In the presently reported experiments, the sample was usually kept at a constant pressure for no more than 10 min, both including the time for pressure stabilization and for data collection, and on this time scale we did not observe any kinetic effect. Indeed, it is difficult to assess the role of kinetics in ILs at high-pressure and its time-scale, and it was not in the scope of present work, but it requires future attention since it has not been deeply investigated to date, besides a few works [14,53,56].

3.3. Computational Results

The vibration frequencies and infrared intensities of the lowest energy configuration of the EMI and TfO ions calculated at the B3LYP/6-31G** level are reported in Table S1 of the Supplementing Information. These results are in good agreement with previous investigations on the same ions [32]. Recently, it has been shown that a good agreement between the calculated and the experimental infrared spectrum of the protic ionic liquid DEMA–TfO can be obtained by exploiting DFT calculations on the ionic couple with the ω B97X-D functional, including empirical dispersion corrections and the presence of a polar solvent (dimethylformamide, $\epsilon_r = 37.22$) [49]. Here, we want to investigate whether this better agreement is visible also in the case of the presently investigated non-protic IL.

Figure 5 reports the optimized geometry of the lowest energy configuration of the EMI–TfO couple with the ω B97X-D functional, considering the presence of a polar solvent. The TfO anion resides above the plane of the imidazolium cation, pointing the O atoms towards the C2 atom of EMI (C atom directly linked to the two N atoms of the imidazolium ion). The calculated distance between the H atom (H2) attached to C2 and the closest O (O1) atom of the anion is 2.23 \AA , a value very close to the value of 2.24 \AA reported for the solid phase of EMI–TfO, as obtained by X-ray diffraction experiments [51]. The calculated angle formed by the C2, H2 and O1 atoms is 136.6° , a value slightly lower than the

experimental value of 149° , which, however, was reported for the solid phase of EMI-TfO [51]. It must be noted that the most evident change induced by considering the presence of a solvent in the DFT calculations is enlargement of the distance between anion and cation in similar ionic couples containing TfO [49], and, indeed, this approach allows to correctly evaluate the H2–O1 distance.

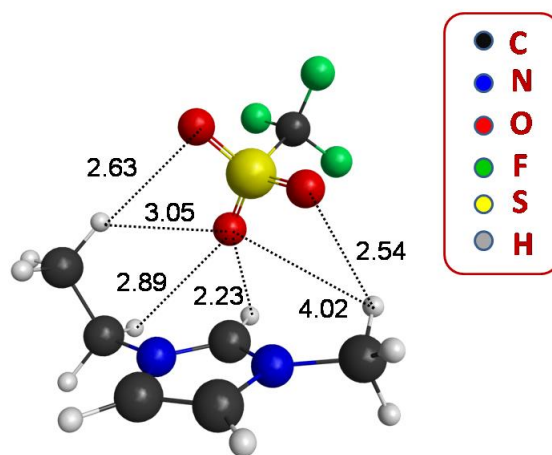


Figure 5. Lowest energy configuration of the EMI-TfO ionic couple, obtained by DFT calculations employing the ω B97X-D functional (including empirical dispersion corrections) and the 6-31G** basis set. The numbers are the distances of selected atoms, expressed in Å.

After optimization of the geometry, the frequencies and intensities of the infrared vibration for the EMI-TfO couple were calculated (see Table S1 of the Supplementing Information). The derived absorbance is compared in Figure 6 with the experimental absorption spectrum at 110 and 330 K and with the calculated absorbance for the single, isolated ions in vacuum. In all cases, no scaling factors for the vibration frequencies were considered.

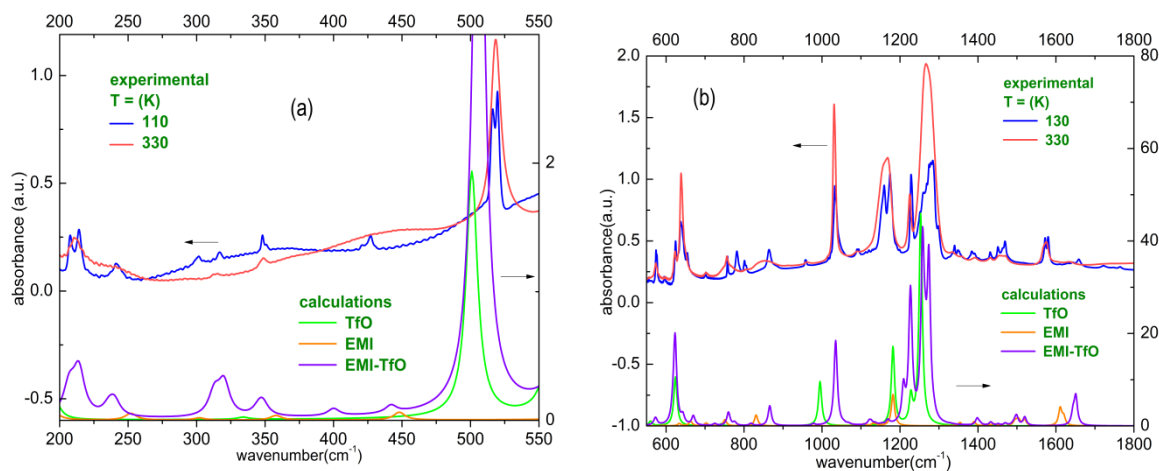


Figure 6. Comparison of the experimental absorbance spectra of EMI-TfO at 110 and 330 K (top part of the panels) with the calculations (bottom part of the panels). For the isolated TfO ion, a frequency scaling factor of 0.97 was used. The panel (a,b) reports the far- (mid-) infrared range.

Comparing the performances of the single ion and ionic couple calculations, one can observe in Figure 6 that the latter can properly account in the far infrared for the two bands between 200 and 220 cm^{-1} , the band around 240 cm^{-1} , the three bands, visible at low temperatures, between 300 and 360 cm^{-1} and the band at 440 cm^{-1} . In addition, the frequency position of the intense band experimentally detected around 520 cm^{-1} is better predicted by the ion couple model. Moreover, in the mid-infrared

range, this last model is able to predict the position and number of bands between 550 and 1100 cm^{-1} . Above such wavenumbers, the strong SO stretching vibrations seems to be concentrated in too narrow a frequency range and, finally, the CH bending modes are shifted to higher frequencies compared to the experiments. This last point is common to all DFT calculations, as CH bending and stretching are highly anharmonic. In general, however, the agreement between the ionic couple model and the experiments is remarkable.

4. Conclusions

The investigation of the infrared absorption spectra of EMI–TfO provided evidence of the phase transition that the material undergoes as a function of temperature or pressure. While, on cooling, the IL crystallizes, no crystallization is observed upon compression, similarly to the case of other ionic liquids that display different behaviors as a function of T and p . Moreover, a new computational investigation of the ionic couple is proposed, obtaining a good description of the experimental infrared spectrum and estimating the distance between the anion and cation to be $\approx 2.23 \text{ \AA}$, in agreement with the value previously reported for the solid phase.

Supplementary Materials: The following are available online at <http://www.mdpi.com/2076-3417/10/12/4404/s1>, Table S1: Infrared vibrational frequencies (ω in cm^{-1}) and intensities (I in km/mol) of the two ions EMI and TfO (calculated by the B3LYP functional and the 6-31G** basis set in a vacuum) and of the EMI–TfO ionic couple (calculated at the ω B97X-D level of theory with the 6-31G** basis set and including a polar medium).

Author Contributions: Conceptualization, A.P., F.C., O.P.; formal analysis, F.T.; investigation, A.P., F.C., O.P., A.C. (Anna Celeste), A.C. (Adriano Cimini); writing—original draft preparation, A.P.; writing—review and editing, all authors; visualization, F.T.; funding acquisition, A.P. All authors have read and agreed to the published version of the manuscript.

Funding: The research leading to this result has been supported by the project CALIPSOplus under the Grant Agreement 730872 from the EU Framework Programme for Research and Innovation HORIZON 2020, for the beamtimes 20170928 and 20190321 at Soleil Synchrotron.

Acknowledgments: We wish to thank P. Roy and J.B. Brubach of the AILES beamline of Soleil Synchrotron for their help during the beamtimes.

Conflicts of Interest: The authors declare no conflict of interest.

References

1. Singh, S.K.; Savoy, A.W. Ionic liquids synthesis and applications: An overview. *J. Mol. Liq.* **2020**, *297*, 112038. [[CrossRef](#)]
2. Kumar, A. A Review on Ionic Liquids as Novel Absorbents for SO_2 Removal. In *Environmental Processes and Management*; Singh, R., Shukla, P., Singh, P., Eds.; Water Science and Technology Library, Springer: Berlin, Germany, 2020; Volume 91, pp. 285–307.
3. Hejazifar, M.; Lanaridi, O.; Bica-Schröder, K. Ionic liquid based microemulsions: A review. *J. Mol. Liq.* **2020**, *303*, 112264. [[CrossRef](#)]
4. Ramos, M.; Jiménez, A.; Garrigós, M.C. IL-based advanced techniques for the extraction of value-added compounds from natural sources and food by-products. *TrAC Trend. Anal. Chem.* **2019**, *119*, 115616. [[CrossRef](#)]
5. Marcinkowska, R.; Konieczna, K.; Marcinkowski, L.; Namieśnik, J.; Kloskowski, A. Application of ionic liquids in microextraction techniques: Current trends and future perspectives. *TrAC Trend. Anal. Chem.* **2019**, *119*, 115614. [[CrossRef](#)]
6. Zandu, S.K.; Chopra, H.; Singh, I. Ionic Liquids for Therapeutic and Drug Delivery Applications. *Curr. Drug Res. Rev.* **2020**, *12*, 26–41. [[CrossRef](#)]
7. Gupta, N.; Liang, Y.N.; Hu, X. Thermally responsive ionic liquids and polymeric ionic liquids: Emerging trends and possibilities. *Curr. Opin. Chem. Eng.* **2019**, *25*, 43–50. [[CrossRef](#)]
8. Usuki, T.; Yoshizawa-Fujita, M. Extraction and Isolation of Natural Organic Compounds from Plant Leaves Using Ionic Liquids. *Adv. Biochem. Eng. Biotechnol.* **2019**, *168*, 227–240.

9. Yang, G.; Song, Y.; Wang, Q.; Zhang, L.; Deng, L. Review of ionic liquids containing, polymer/inorganic hybrid electrolytes for lithium metal batteries. *Mater. Des.* **2020**, *190*, 108563. [[CrossRef](#)]
10. Navarra, M.A. Ionic Liquids as Safe Electrolyte Components for Li-Metal and Li-Ion Batteries. *MRS Bull.* **2013**, *38*, 548–553. [[CrossRef](#)]
11. Palumbo, O.; Trequattrini, F.; Appetecchi, G.B.; Paolone, A. The influence of the alkyl chain length on the microscopic configurations of the anion in the crystalline phases of PYR_{1A}-TFSI. *J. Phys. Chem. C* **2017**, *121*, 11129–11135. [[CrossRef](#)]
12. Paschoal, V.H.; Faria, L.F.O.; Ribeiro, M.C.C. Vibrational spectroscopy of ionic liquids. *Chem. Rev.* **2017**, *117*, 7053–7112. [[CrossRef](#)] [[PubMed](#)]
13. Yoshimura, Y.; Takekiyo, T.; Imai, Y.; Abe, H. Pressure-induced spectral changes of room-temperature ionic liquid, N,N-diethyl-N-methyl-N-(2-methoxyethyl)ammonium bis(trifluoromethylsulfonyl)imide, [DEME][TFSI]. *J. Phys. Chem. C* **2012**, *116*, 2097–2101. [[CrossRef](#)]
14. Yoshimura, Y.; Abe, H.; Imai, Y.; Takekiyo, T.; Hamaya, N. Decompression-induced crystal polymorphism in a room-temperature ionic liquid, N,N-diethyl-N-methyl-N-(2-methoxyethyl) ammonium tetrafluoroborate. *J. Phys. Chem. B* **2013**, *117*, 3264–3269. [[CrossRef](#)] [[PubMed](#)]
15. Zhu, X.; Yuan, C.; Li, H.; Zhu, P.; Su, L.; Yang, K.; Wu, J.; Yang, G.; Liu, J. Successive disorder to disorder phase transitions in ionic liquid under high pressure. *J. Mol. Struct.* **2016**, *1106*, 70–75. [[CrossRef](#)]
16. Faria, L.F.O.; Lima, T.A.; Ribeiro, M.C.C. Phase transitions of the ionic liquid [C2C1im][NTf2] under high pressure: A synchrotron X-ray diffraction and Raman microscopy study. *Cryst. Growth Des.* **2017**, *17*, 5384–5392. [[CrossRef](#)]
17. Chen, F.; You, T.; Yuan, Y.; Pei, C.; Ren, X.; Huang, Y.; Yu, Z.; Li, X.; Zheng, H.; Pan, Y.; et al. Pressure-induced structural transitions of a room temperature ionic liquid—1-ethyl-3- methylimidazolium chloride. *J. Chem. Phys.* **2017**, *146*, 094502. [[CrossRef](#)]
18. Abe, H.; Kishimura, H.; Takaku, M.; Watanabe, M.; Hamaya, N. Low-temperature and high-pressure phases of a room-temperature ionic liquid and polyiodides: 1-methyl-3-propylimidazolium iodide. *Faraday Discuss.* **2018**, *206*, 49–60. [[CrossRef](#)]
19. Faria, L.F.O.; Nobrega, M.M.; Falsini, N.; Fanetti, S.; Temperini, M.L.A.; Bini, R.; Ribeiro, M.C.C. Structure and Reactivity of the Ionic Liquid 1-Allyl-3-methylimidazolium Iodide under High Pressure. *J. Phys. Chem. B* **2019**, *123*, 1822–1830. [[CrossRef](#)]
20. Penna, T.C.; Ribeiro, M.C.C. Vibrational frequency shift of 1-alkyl-3-methylimidazolium tetrafluoroborate ionic liquids under high pressure. *J. Mol. Liq.* **2019**, *278*, 213–218. [[CrossRef](#)]
21. Wu, J.; Cheng, X.; Wu, M.; Li, H.; Zhu, X.; Wang, Z.; Yuan, C.; Yang, K.; Su, L. Crystallization of ionic liquid [EMIM][NO₃] under extreme conditions. *J. Mol. Struct.* **2019**, *1189*, 265–271. [[CrossRef](#)]
22. Osti, N.C.; Haberl, B.; Jalarvo, N.; Boehler, R.; Molaison, J.J.; Goyette, R.J., Jr.; Mamontov, E. Dynamics of a room temperature ionic liquid under applied pressure. *Chem. Phys.* **2020**, *530*, 110628. [[CrossRef](#)]
23. Capitani, F.; Gatto, S.; Postorino, P.; Palumbo, O.; Trequattrini, F.; Deutsch, M.; Brubach, J.-B.; Roy, P.; Paolone, A. The complex dance of the two conformers of bis(trifluoromethanesulfonyl)-imide as a function of pressure and temperature. *J. Phys. Chem. B* **2016**, *120*, 1312–1318. [[CrossRef](#)] [[PubMed](#)]
24. Capitani, F.; Trequattrini, F.; Palumbo, O.; Paolone, A.; Postorino, P. Phase transitions of PYR₁₄-TFSI as a function of pressure and temperature: The competition between smaller volume and lower energy conformer. *J. Phys. Chem. B* **2016**, *120*, 2921–2928. [[CrossRef](#)] [[PubMed](#)]
25. Capitani, F.; Trequattrini, F.; Palumbo, O.; Roy, P.; Postorino, P.; Paolone, A. Pressurizing the mixtures of two ionic liquids: Crystallization vs. vitrification. *J. Raman Spectr.* **2017**, *48*, 1819–1827. [[CrossRef](#)]
26. Faria, L.F.O.; Nobrega, M.M.; Temperini, M.L.A.; Bini, R.; Ribeiro, M.C.C. Triggering the chemical instability of an ionic liquid under high pressure. *J. Phys. Chem. B* **2016**, *120*, 9097–9102. [[CrossRef](#)]
27. Capitani, F.; Höppner, M.; Malavasi, L.; Marini, C.; Artioli, G.A.; Hanfland, M.; Dore, P.; Boeri, L.; Postorino, P. Structural evolution of solid phenanthrene at high pressures. *J. Phys. Chem. C* **2016**, *120*, 14310–14316. [[CrossRef](#)]
28. Izgorodina, E.I.; Seeger, Z.L.; Scarborough, D.L.A.; Tan, S.Y.S. Quantum Chemical Methods for the Prediction of Energetic, Physical, and Spectroscopic Properties of Ionic Liquids. *Chem. Rev.* **2017**, *117*, 6696–6754. [[CrossRef](#)]
29. Dong, K.; Liu, X.; Dong, H.; Zhang, X.; Zhang, S. Multiscale studies on ionic liquids. *Chem. Rev.* **2017**, *117*, 6636–6695. [[CrossRef](#)]

30. Herstedt, M.; Smirnov, M.; Johansson, P.; Chami, M.; Grondin, J.; Servant, L.; Lassègues, J.C. Spectroscopic characterization of the conformational states of the bis(trifluoromethanesulfonyl)imide Anion (TFSI⁻). *J. Raman Spectrosc.* **2005**, *36*, 762–770. [[CrossRef](#)]
31. Fujii, K.; Seki, S.; Fukuda, S.; Kanzaki, R.; Takamuku, T.; Umebayashi, Y.; Ichiguro, S.-I. Anion conformation of low-viscosity room-temperature ionic liquid 1-ethyl-3-methylimidazolium bis(fluorosulfonyl) imide. *J. Phys. Chem. B* **2007**, *111*, 12829–12833. [[CrossRef](#)]
32. Umebayashi, Y.; Fujimori, T.; Sukizaki, T.; Asada, M.; Fujii, K.; Kanzaki, R.; Ishiguro, S.-I. Evidence of Conformational Equilibrium of 1-Ethyl-3-methylimidazolium in Its Ionic Liquid Salts: Raman Spectroscopic Study and Quantum Chemical Calculations. *J. Phys. Chem. A* **2005**, *109*, 8976–8982. [[CrossRef](#)]
33. Haddad, B.; Paolone, A.; Villemin, D.; Taqiyeddine, M.; Belarbi, E.; Bresson, S.; Rahmouni, M.; Dhupal, N.R.; Kim, H.J.; Kiefer, J. Synthesis, conductivity, and vibrational spectroscopy of tetraphenylphosphonium bis(trifluoromethanesulfonyl)imide. *J. Mol. Struct.* **2017**, *1146*, 203–212. [[CrossRef](#)]
34. Palumbo, O.; Vitucci, F.M.; Trequatrini, F.; Paolone, A. A study of the conformers of the N,N-diethyl-N-methyl-N-propylammonium ion by means of infrared spectroscopy and DFT calculations. *Vib. Spec.* **2015**, *80*, 11–16. [[CrossRef](#)]
35. Singh, D.K.; Rathke, B.; Kiefer, J.; Materny, A. Molecular structure and interactions in the ionic liquid 1-ethyl-3-methylimidazolium trifluoromethanesulfonate. *J. Phys. Chem. A* **2016**, *120*, 6274–6286. [[CrossRef](#)]
36. Panja, S.; Haddad, B.; Debdbad, M.; Kiefer, J.; Chaker, Y.; Bresson, S.; Paolone, A. Cluster formation through hydrogen bond bridges across chloride anions in a hydroxyl-functionalized ionic liquid. *ChemPhysChem* **2019**, *20*, 936–940. [[CrossRef](#)] [[PubMed](#)]
37. Fumino, K.; Fossog, V.; Wittler, K.; Hempelmann, R.; Ludwig, R. Dissecting anion-cation interaction energies in protic ionic liquids. *Angew. Chem. Int. Ed.* **2013**, *52*, 2368–2372. [[CrossRef](#)]
38. Fumino, K.; Reichert, E.; Wittler, K.; Hempelmann, R.; Ludwig, R. Low-frequency vibrational modes of protic molten salts and ionic liquids: Detecting and quantifying hydrogen bonds. *Angew. Chem. Int. Ed.* **2012**, *51*, 6236–6240. [[CrossRef](#)]
39. Fumino, K.; Fossog, V.; Stange, P.; Paschek, D.; Hempelmann, R.; Ludwig, R. Controlling the subtle energy balance in protic ionic liquids: Dispersion forces compete with hydrogen bonds. *Angew. Chem. Int. Ed.* **2015**, *54*, 2792–2795. [[CrossRef](#)]
40. Niemann, T.; Zaitsau, D.H.; Strate, A.; Stange, P.; Ludwig, R. Controlling “like–likes–like” charge attraction in hydroxy-functionalized ionic liquids by polarizability of the cations, interaction strength of the anions and varying alkyl chain length. *Phys. Chem. Chem. Phys.* **2020**, *22*, 2763–2774. [[CrossRef](#)] [[PubMed](#)]
41. Dong, K.; Song, Y.; Liu, X.; Cheng, W.; Yao, X.; Zhang, S. Understanding structures and hydrogen bonds of ionic liquids at the electronic level. *J. Phys. Chem. B* **2012**, *116*, 1007–1017. [[CrossRef](#)]
42. Liu, Z.; El Abedinab, S.Z.; Endres, F. Electrochemical and spectroscopic study of Zn(II)coordination and Zn electrodeposition in three ionic liquids with the trifluoromethylsulfonate anion, different imidazolium ions and their mixtures with water. *Phys. Chem. Chem. Phys.* **2015**, *17*, 15945–15952. [[CrossRef](#)] [[PubMed](#)]
43. Vygodskii, Y.S.; Mel’nik, O.A.; Lozinskaya, E.I.; Shaplov, A.S.; Malyshkina, I.A.; Gavrilova, N.D.; Lyssenko, K.A.; Antipin, M.Y.; Golovanov, D.G.; Korlyukov, A.A.; et al. The influence of ionic liquid’s nature on free radical polymerization of vinyl monomers and ionic conductivity of the obtained polymeric materials. *Polym. Adv. Technol.* **2007**, *18*, 50–63. [[CrossRef](#)]
44. Ignat’ev, N.V.; Barthen, P.; Kucheryna, A.; Willner, H.; Sartori, P. A convenient synthesis of triflate anion ionic liquids and their properties. *Molecules* **2012**, *17*, 5319–5338. [[CrossRef](#)] [[PubMed](#)]
45. Faye, M.; Bordessoule, M.; Kanouté, B.; Brubach, J.B.; Roy, P.; Manceron, L. Improved mid infrared detector for high spectral or spatial resolution and synchrotron radiation use. *Rev. Sci. Instr.* **2016**, *87*, 063119. [[CrossRef](#)] [[PubMed](#)]
46. Celeste, A.; Borondics, F.; Capitani, F. Hydrostaticity of pressure-transmitting media for high pressure infrared spectroscopy. *High Pres. Res.* **2019**, *39*, 608–618. [[CrossRef](#)]
47. Piermarini, G.J.; Block, S.; Barnett, J.D.; Forman, R.A. Calibration of the Pressure Dependence of the R1 Ruby Fluorescence Line to 195 Kbar. *J. Appl. Phys.* **1975**, *46*, 2774–2780. [[CrossRef](#)]
48. Shao, Y.; Molnar, L.F.; Jung, Y.; Kussmann, J.; Ochsenfeld, C.; Brown, S.T.; Gilbert, A.T.B.; Slipchenko, L.V.; Levchenko, S.V.; O’Neill, D.P.; et al. Advances in methods and algorithms in a modern quantum chemistry program package. *Phys. Chem. Chem. Phys.* **2006**, *8*, 3172–3191. [[CrossRef](#)] [[PubMed](#)]

49. Palumbo, O.; Cimini, A.; Trequattrini, F.; Brubach, J.-B.; Roy, P.; Paolone, A. The infrared spectra of protic ionic liquids: Performances of different computational models to predict hydrogen bonds and conformer evolution. *Phys. Chem. Chem. Phys.* **2020**, *22*, 7497–7506. [[CrossRef](#)]
50. Kiefer, J.; Stuckenholtz, M.; Rathke, B. Influence of the alkyl chain on the vibrational structure and interionic interactions in 1-alkyl-3-methylimidazolium trifluoromethanesulfonate liquids. *J. Mol. Liq.* **2018**, *255*, 413–418. [[CrossRef](#)]
51. Choudhury, A.R.; Winterton, N.; Steiner, A.; Cooper, A.I.; Johnson, K.A. In situ crystallization of ionic liquids with melting points below $-25\text{ }^{\circ}\text{C}$. *CrystEngComm* **2006**, *8*, 742–745. [[CrossRef](#)]
52. Faria, L.F.O.; Ribeiro, M.C.C. Phase transitions of triflate-based ionic liquids under high pressure. *J. Phys. Chem. B* **2015**, *119*, 14315–14322. [[CrossRef](#)] [[PubMed](#)]
53. Chen, L.; Li, H.; Zhu, X.; Su, L.; Yang, K.; Yuan, C.; Yang, G.; Li, X. Structural and conformational properties of 1-decyl-3-methylimidazoliumtetrafluoroborate under high pressure. *J. Mol. Struct.* **2017**, *1137*, 610–614. [[CrossRef](#)]
54. Li, H.; Wang, Z.; Chen, L.; Huang, H.; Wu, J.; Huang, H.; Yang, K.; Wang, Y.; Su, L.; Yang, G. Kinetic Effect on Pressure-Induced Phase Transitions of Room Temperature Ionic Liquid, 1-Ethyl-3-methylimidazolium Trifluoromethanesulfonate. *J. Phys. Chem. B* **2015**, *119*, 14245–14251. [[CrossRef](#)] [[PubMed](#)]
55. Burba, C.M.; Chang, H.-C. Temperature- and pressure-dependent infrared spectroscopy of 1-butyl-3-methylimidazolium trifluoromethanesulfonate: A dipolar coupling theory analysis. *Spectr. Acta A Mol. Biomol. Spectr.* **2018**, *193*, 338–343. [[CrossRef](#)]
56. Su, L.; Li, M.; Zhu, X.; Wang, Z.; Chen, Z.; Li, F.; Zhou, Q.; Hong, S. In Situ Crystallization of Low-Melting Ionic Liquid [BMIM][PF₆] under High Pressure up to 2 GPa. *J. Phys. Chem. B* **2013**, *117*, 12296–12302. [[CrossRef](#)]



© 2020 by the authors. Licensee MDPI, Basel, Switzerland. This article is an open access article distributed under the terms and conditions of the Creative Commons Attribution (CC BY) license (<http://creativecommons.org/licenses/by/4.0/>).